

## Effect of Stress Concentration on Magnetic Flux Leakage Signals from Blind-Hole Defects in Stressed Pipeline Steel

T. W. Krause, R. W. Little, R. Barnes, R. M. Donaldson, B. Ma, and D. L. Atherton

Department of Physics, Queen's University, Kingston, Ontario, K7L 3N6, Canada

**Abstract.** Stress-dependent magnetic flux leakage (MFL) signals of the normal surface component (radial) MFL signal from blind-hole defects in pipeline steel were investigated. Three different stress rigs with uniaxial stress and field configurations were used. A double-peak feature in the MFL signal was defined quantitatively by a saddle amplitude, which was taken as the difference between the average of the double peaks and the corresponding saddle point. Results indicated that the saddle amplitude increased linearly with increasing tensile surface stress and decreased, or did not exist, for increasing compressive surface stress. The stress-dependent saddle amplitude was shown to increase with increasing defect depth. Finite-element calculations indicated that stress concentration also increased with increasing defect depth. The measurements and analysis demonstrate that the stress-dependent saddle amplitude behavior in the radial MFL signal is associated with surface-stress concentrations near the blind-hole defects.

### Introduction

Magnetic flux leakage (MFL) techniques are commonly used for the in-line inspection of pipelines for metal loss defects such as corrosion pits [1]. The in-service operating pressures of gas pipelines generate large circumferential stresses that may reach 70% of the yield strength of the pipe. These in-service stresses affect the flux leakage patterns and have been studied previously [2]–[7]. In the presence of stress, defects act as “stress raisers” [8]. Dependent upon the defect depth [9], the defects may generate stress concentrations that exceed the yield strength in their vicinity. Stress raising around defects also may lead to enhanced stress corrosion cracking [10].

There are two effects that may contribute to the generation of the stress-dependent MFL signal: 1) the bulk effect of stress on the magnetic properties [11]–[16] and 2) the effect of the defect as a stress raiser that is also dependent on the depth of the defect [9]. Metal loss resulting from increasing defect depth increases the level of magnetic saturation in the vicinity of the defect and, therefore, increases the MFL signal. Similarly, by affecting the stress-dependent magnetic properties of the steel in the vicinity of the defect, the application of a bulk stress also affects the peak-to-peak MFL ( $MFL_{pp}$ ) signal. Stress concentrations in the vicinity of the defect have a similar effect. From a previous consideration [17], under a bending stress the two-dimensional solution for a 100% through-wall defect or hole generates a peak stress level at the edge of the

hole that is 2.4 times that of the nominal background stress [8, 17]. Finite-element calculations and stress measurements [17] indicate that, for the same bending stress, the stress concentration for a round-bottomed pit that is 50% of the through-wall thickness is 1.2 times the nominal stress. For a plate under uniform tensile stress, the maximum stress at the edge of a full cylindrical through-hole is three times that of the nominal stress [8, 18]. Stress concentrations occur at the two edges of the defect that are tangential to the applied stress direction.

An increase in the pipe wall flux density typically results in an increase in the MFL signal due to increased saturation of the steel in the defect region. The effect of stress on the MFL<sub>pp</sub> signal has been shown to increase for increasing flux densities in the range of 0.65 to 1.24 T [9, 13]–[16]. It is expected, therefore, that stress concentration combined with increasing flux density may similarly affect the MFL signal.

Observations of a double-peak feature that increases in amplitude with increasing applied tensile stress have been made for normal-surface component (radial) MFL signals for various uniaxial orientations of stress and field applied to pipeline steel [5, 11]. In particular, the amplitude of the double-peak feature (hereafter referred to as the saddle amplitude) has been observed to increase linearly with increasing levels of applied stress and has been associated with stress patterns around the defect itself [12, 14]. In this paper we provide evidence that strongly supports this claim. Further, it is demonstrated that the double-peak feature in the MFL signal may be associated primarily with stress concentrations that appear in the vicinity of the defect near the surface of the steel pipeline sample, and also that the stress concentration and resultant saddle amplitude in the MFL signal increase with increasing defect depth.

## Experimental Apparatus

The experimental apparatus is described in detail elsewhere [11, 12]. The apparatus used to measure the radial component of the flux leakage field from a defect on the same side of the sample as the measuring apparatus (near side) consisted of a Hall probe, an amplifier to amplify the Hall signal, and a computer for data acquisition. The radial flux leakage signal was measured at scanned positions set at 1-mm intervals (0.5 mm for the semicircular pipe section) across the area of the defect. The radial flux leakage signal was taken as the average of 100 measurements taken at each position.

### *Pipeline Sample and Stressing Apparatus*

Samples of pipeline steel used in this study were cut from a 610-mm (24-in.) diameter X70 steel pipe of 9-mm wall thickness. The first sample used was a 102-mm (4-in.) wide semicircular section cut in the pipe hoop direction. Other samples used were 4.27-m long axial strips that were also 102 mm (4 in.) wide. The pipeline steel composition is given elsewhere [17].

There were three separate experimental test rigs. The first apparatus is the semicircular hoop bending rig shown in Fig. 1. The second and third apparatus use the single-strip beam-bending arrangement and the composite beam-bending arrangement,

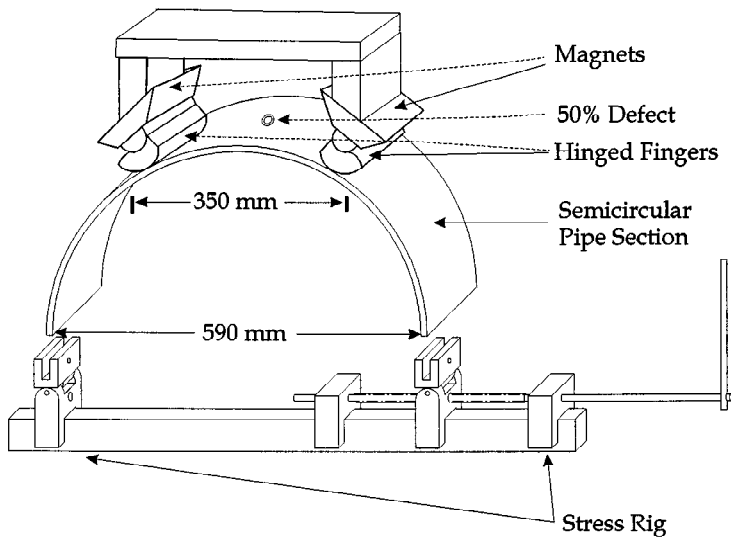


**Fig. 1.** The semicircular pipe section and bending stress rig for the production of surface stress in semicircular sections of pipe steel.

both described elsewhere [11, 12]. Surface stresses up to  $\pm 300$  MPa were applied using the three stress rigs. This is below the yield stress of the pipe steel, which is at 500 MPa. All three sets of apparatus have a 13-mm diameter ball-milled external pit machined to 50% of the steel wall thickness. The composite beam apparatus also has two more 13-mm diameter ball-milled external pits machined to depths of 25 and 75%. An area of about 40 mm by 40 mm around the defect was stripped of its epoxy coating to expose the pipe steel. The defect area was magnetized to a maximum axial flux density of 1.6 T using ferrite magnets. For the semicircular pipe section, steel hinged fingers were used to couple the flux from the magnets into the steel pipe, while for the two beams, steel brushes shaped to the curvature of the beams coupled flux into the steel samples.

### *Semicircular Pipe Section Stress Rig*

In the first stress rig, shown in Fig. 1, a semicircular pipe section is held stationary by a fixed clamp, while the other is connected to a movable clamp. The movable clamp is free to travel along a horizontal threaded rod as the rod is rotated with the handle, the result being the application of a hoop-bending stress. When the clamp is moved inward, tension is created on the outside and compression on the inside pipe surface, with the opposite being true if the clamp were to be moved outward. A “clamp position versus stress” calibration was obtained theoretically [17] and verified using strain gauges (placed well away from the defect region).

### *Single Beam*

The single-strip beam is a 102-mm wide strip of steel cut in the axial direction from the 610-mm diameter pipe with a thickness of 9 mm and a length of 4.27 m. The low rigidity of the single beam allows bending by simply hanging masses of about 5 kg from one end of the beam or supporting it at a raised height while the middle length of the beam is supported and the opposite end of the beam is fixed in position.

### *Composite Beam*

The third apparatus utilizes a composite beam and an arrangement to bend the beam [11, 12]. The composite beam is made from two axial strips of pipeline steel that are separated at a fixed distance of 29 mm by an alternating fiberglass–wood composite. The composite materials are bonded together with high-strength epoxy resin. Under a bending stress the neutral axis of the beam is outside the pipeline steel regions, so that nearly uniform stress is generated through the thickness of the steel walls. Because the composite beam is much more rigid, the beam is stressed by placing it parallel to a comparably rigid pipe section of equal length separated by a wood saddle in the middle. At one end the beam and pipe are held together by a clamp or chain, and at the other end the beam and pipe are pulled together by another clamp with a scissor jack. For tests using tensile stress the steel strip with the defect in it is on the side facing away from the rigid pipe, with the composite beam above the pipe. For compressive stress the steel strip is on the side facing toward the pipe and with the beam underneath the pipe, so that the detector can be placed on top of the beam.

### *Stress Cycles*

Three different procedures of applying field and stress are used to perform the measurements: 1) the “normal cycle,” which involves magnetizing the beam with no applied stress and maintaining the applied field during the stressing of the beam; 2) the “opposite cycle,” which is similar to the “normal cycle” except that the magnetization is generated with the field in the opposite polarity; and 3) the “after-cycle,” which involves removing the magnet before each stressing increment and then replacing it so that the beam is remagnetized after each change of stress. In all three methods, the defects are scanned at fixed levels of stress. Of the three cycles, the after-cycle is the most similar to an actual pipeline pigging measurement.

Measurements of the peak-to-peak magnetic flux leakage (MFL<sub>pp</sub>) signal in the normal-cycle mode across a 50% penetration round-bottomed blind-hole–simulated defect for various levels of applied tensile and compressive stress in the semicircular pipe section were performed using the hoop-bending stress rig shown in Fig. 1. Starting from 0 MPa, tensile stress up to 250 MPa was applied followed by changes in stress to 250 MPa compressive stress and, finally, back to a 0-MPa stress level. The MFL signal was recorded at various levels of applied stress. The stress in the pipe section was adjusted by varying the distance between the ends of the semicircular pipe section in the stress rig to various strain gauge calibrated settings.

For the composite beam tensile stress scans were performed, first for all three defects and stress cycles, and then followed by compressive stress scans, since a reorientation of the beam was required. No compressive stress scans were performed for the single beam.

#### *Variation of Pipeline Steel Flux Density*

The total flux density within the semicircular pipe section was measured by removing the magnetizing system, noting the flux change, reversing the polarity of the magnetizer, applying it again, and noting the flux change again. The average of the two flux readings was taken and the flux density within the pipe and was found to be 1.54 T. The total flux density within the single-beam stress rig was determined in the same manner and was found to be 1.6 T.

Two techniques were used to vary the flux density within the composite beam pipe wall and are described in detail elsewhere [9, 13]. The first technique consisted of changing the size of the magnets used, and the second involved the application of partial shorting bars. The steel bars diverted some of the flux from the magnets and therefore reduced the flux density in the pipe wall. An integrating voltage fluxmeter, connected to a 13-turn coil wound around one section of steel beam and through a hole in the center of the composite beam assembly, was used to determine the flux density within the pipe wall. The four pipe wall flux densities generated within the composite beam pipe wall using these two techniques were 0.65 T, 0.84 T, 1.03 T, and 1.24 T.

#### *Analysis*

The peak-to-peak radial component of the magnetic flux leakage ( $MFL_{pp}$ ) signal is obtained by taking the difference between the maximum (positive) and minimum (negative) components of the MFL signal. Positive saddle amplitude values are obtained from the MFL signal by evaluating the difference between the average of the two positive peaks and the positive saddle point. Negative saddle amplitude values are obtained in the same manner, except that the negative double MFL peaks and the negative saddle point are used for the evaluation. Both the variation of the  $MFL_{pp}$  signal and the saddle amplitude as functions of stress were investigated.

#### *Finite-Element Calculations*

A three-dimensional finite-element method was used to model the stress pattern surrounding the defect. Finite-element modeling was performed using the ANSYS Revision 4.4 by Swanson Analysis Systems. A ten-node tetrahedral element with three directional degrees of freedom at each node was used to mesh the solid model. The volumes were defined using a solid modeling approach, where the geometry of the object was described by specifying key points, lines, areas, and volumes. ANSYS then filled in the solid model with nodes and elements based on the user-defined element shape and size.

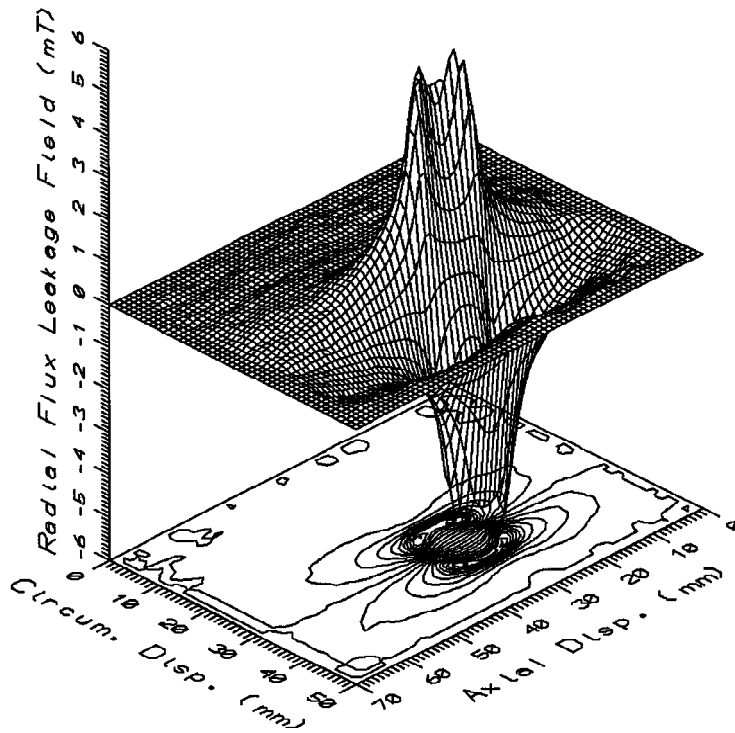


**Fig. 2.** (a) Surface and contour plots of the radial magnetic flux leakage from the near side of a 13-mm-diameter ball-milled 50% defect in the semicircular pipe section under a tensile stress of 250 MPa during a normal cycle.

The finite-element calculations modeled a flat plate with a ball-milled defect. The plate dimensions were taken as 50 mm  $\times$  50 mm with a thickness of 9 mm, which was the same as that of the pipeline steel samples. The radius of curvature of the ball-mill that generated the defect was taken as 6.35 mm. The full defect radius was, therefore, only attained at 71% defect depth. This may have affected the calculations since the defect radius was changing continuously with respect to the mesh distribution up to 71% of the wall thickness. Young's modulus was taken as 210 GPa and Poisson's ratio as 0.28. Calculations were performed for a nominal stress of 190 MPa.

## Results

### *Semicircular Pipe Section: $MFL_{pp}$ Measurements*

Figures 2a and 2b show surface and contour plots of the radial magnetic flux density leakage field over the defect for tensile and compressive stresses of 250 MPa, respectively.

Both scans are from the normal-cycle procedure using constant magnetization. The amplitude of a signal is obtained by taking the difference between the maximum and

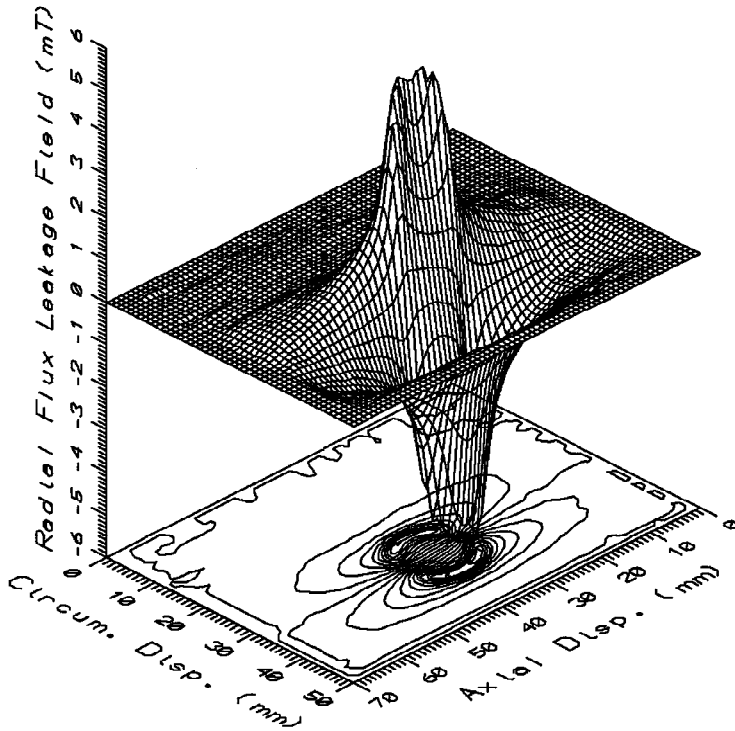


**Fig. 2.** (b) Surface and contour plots of the radial magnetic flux leakage from the near side of a 13-mm-diameter ball-milled pit in the semicircular pipe section under compressive stress at 250 MPa during a normal cycle.

minimum values of flux density over the area of the scan ( $MFL_{pp}$ ). The profile of the contours is typical for all scans, with slight variations with changing stress. Comparing the two scans, a more pronounced double-peak feature is observed for the tensile surface stress case than for the compressive surface stress case.

The  $MFL_{pp}$  signal as a function of stress for the semicircular pipe section under bending-hoop stress is shown in Fig. 3. Starting at 0 MPa, the variation of the  $MFL_{pp}$  signal with surface stress demonstrates an initial increase with the application of tensile stress followed by a decrease and a large hysteresis loop as the stress is cycled from 250 MPa to  $-250$  MPa. Under a compressive stress the variation of the  $MFL_{pp}$  signal is smaller, as is the hysteresis. The final zero-stress  $MFL_{pp}$  signal is greater than the initial starting point. Arrows indicate the order in which the data were taken.

#### *Variation of Saddle Amplitude with Stress*

Results obtained from an analysis of the positive and negative saddle amplitudes as a function of surface stress in the normal cycle are shown for the semicircular pipe section in Fig. 4. Positive and negative saddle amplitudes are present for the zero-stress case.

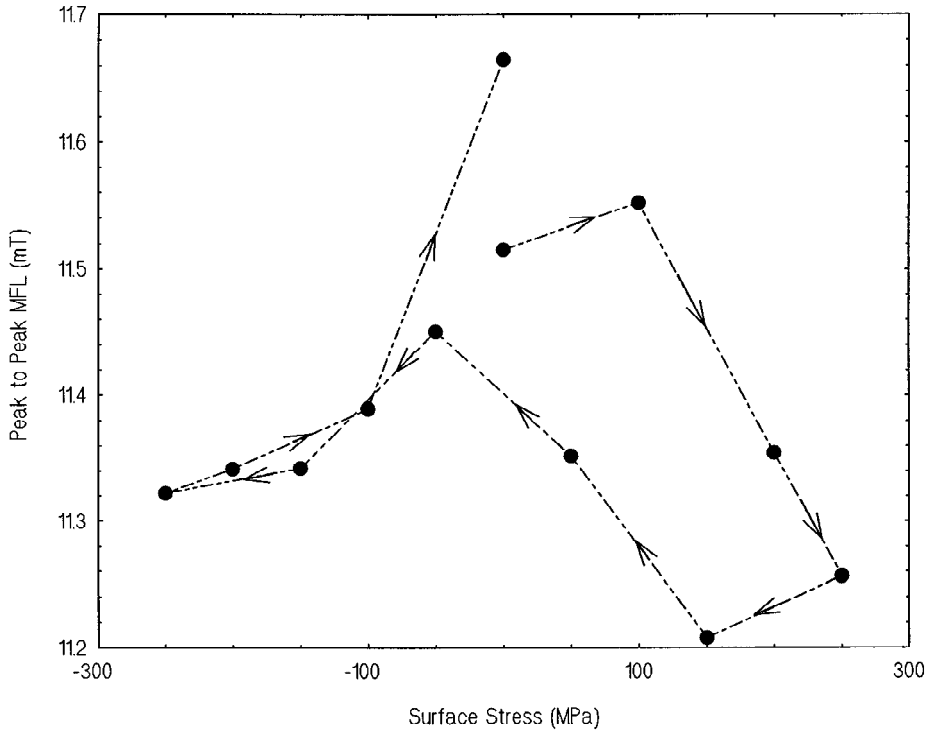


**Fig. 3.** Peak-to-peak MFL signal from the near side as a function of surface stress in the normal cycle for a 13-mm-diameter ball-milled 50% defect on the semicircular pipe section under hoop-bending stress with an applied pipe wall flux density of 1.54 Tesla at 0 MPa.

Since hysteresis is present, arrows indicate the direction in which the data were taken. The positive saddle amplitude increases linearly from a minimum at 250 MPa compressive stress to a maximum at 200 MPa tensile stress. Some hysteresis is evident. In comparison, the negative saddle amplitude is smaller in magnitude, more hysteretic, and slightly less linear.

For the single-beam stress rig, observations of a saddle amplitude that depended linearly on stress were made for tensile surface stress measurements equal to and greater than 200 MPa measured in the normal cycle. In this rig a saddle was not observed for zero or applied compressive stresses. As in the semicircular pipe section, the magnitude of the positive saddle amplitudes was greater than the corresponding negative saddle amplitudes.

The variations of the positive and negative saddle amplitudes with stress for the composite beam for the three defect depths in the normal cycle at 1.24 T are shown in Fig. 5 for tensile stress values. For the composite beam no saddle was observed for any zero or compressive stress values, which is in contrast to the semicircular pipe section where a saddle amplitude that was a decreasing function of increasing compressive stress was observed. This result is considered further in the discussion. The results for the composite beam indicate an increasing variation of saddle amplitude with stress for

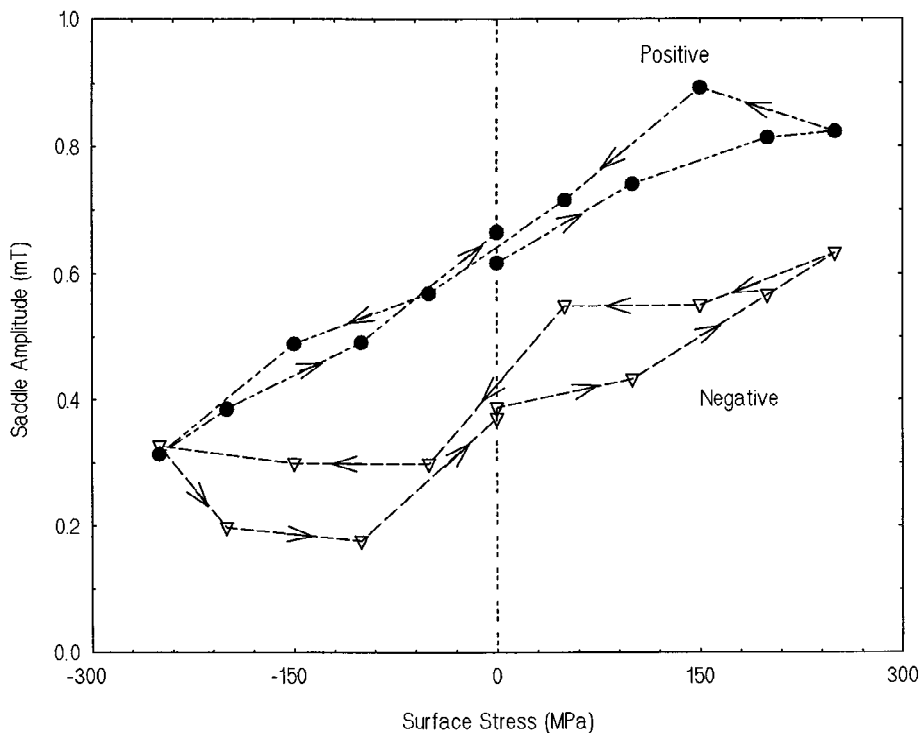


**Fig. 4.** Positive (●) and negative (▽) saddle amplitudes as functions of surface stress using the semi-circular pipeline apparatus with a field of 1.54 T during the normal cycle are plotted for the 13-mm ball-milled 50% defect.

increasing defect depth. For the 25 and 50% depth defects the positive saddle amplitudes are greater in magnitude than the negative saddle amplitude values for equivalent levels of stress, while at 75% this difference is not as great.

The dependence of the positive and negative saddle amplitudes upon stress in the composite beam for the three different defect depths for measurements performed in the after-cycle at 1.24 T are shown in Fig. 6. In contrast to the normal-cycle measurements for the 25 and 50% defects, the magnitude of the negative saddle amplitudes is greater than that of the positive saddle amplitudes, while there is no observed difference between the magnitudes for the 75% defect. The rate of change of the saddle amplitude with stress is greatest for the 75% defect and least for the 25% defect.

#### *Stress-Dependent Saddle Amplitude Slopes*

Linear best fits were applied to the saddle amplitude data as a function of stress for the three different stress rigs. The slopes of saddle amplitude variation with stress for the normal cycle in the three different stress rigs are shown in Table 1. Several observations can be made for the normal-cycle stress applied in the three different stress rigs. These

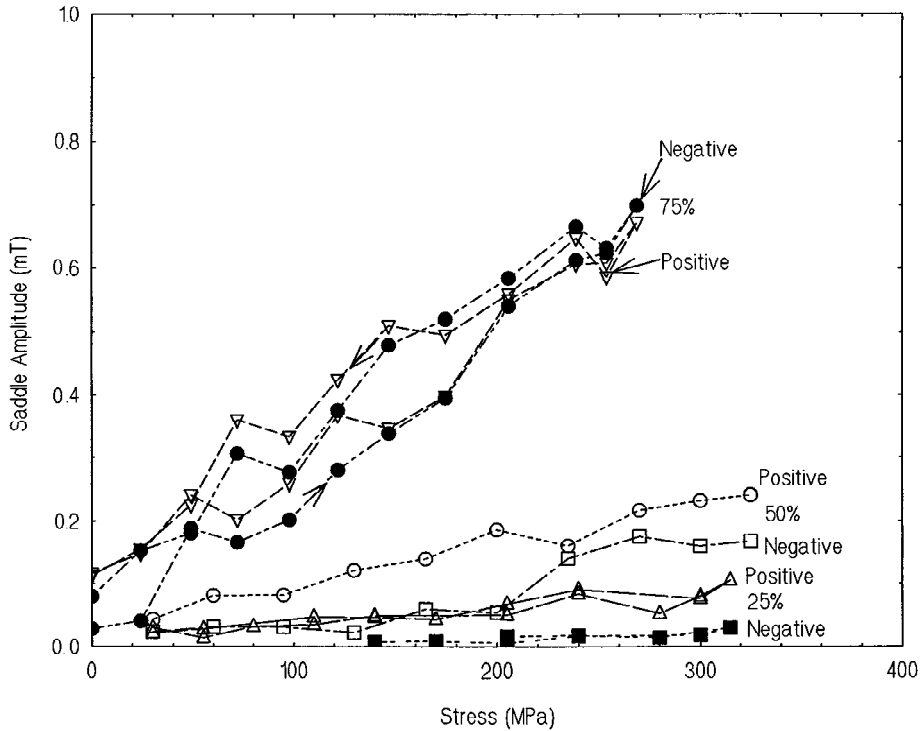


**Fig. 5.** Saddle amplitudes as a function of stress in the composite beam apparatus from 13-mm ball-milled defects in a field of 1.24 T in the normal cycle are plotted for the 25% defect for the positive ( $\Delta$ ) and negative ( $\blacksquare$ ), for the 50% defect for the positive ( $\circ$ ) and negative ( $\square$ ), and for the 75% defect for the positive ( $\nabla$ ) and negative ( $\bullet$ ) saddle amplitudes.

**Table 1.** Best fit slopes for normal-cycle  $MFL_{pp}$  and saddle amplitude with different defect depths in the composite beam and 50% defect in the semicircular pipe section and single beam.

% Defect depth	$MFL_{pp}$ stress slope ( $10^{-12}$ T/Pa)	vs. Stress-dependent saddle amplitude pos. ( $10^{-13}$ T/Pa)	Stress-dependent saddle amplitude neg. ( $10^{-13}$ T/Pa)	+Sad. amp. $MFL_{pp}$ slope (= col.3/col.2)	-Sad. amp. $MFL_{pp}$ slope (= col.4/col.2)
Composite Beam ( $B = 1.24$ T)					
25%	1.6	2	1	0.13	0.06
50%	5.1	7	6	0.14	0.12
75%	11.0	19.1	19.5	0.174	0.177
Semicircular Pipe Section ( $B = 1.54$ T)					
50%	—	11	8	—	—
Single Beam ( $B = 1.6$ T)					
50%	2.3	1.6	$8 \pm 3$	$9 \pm 3$	0.35

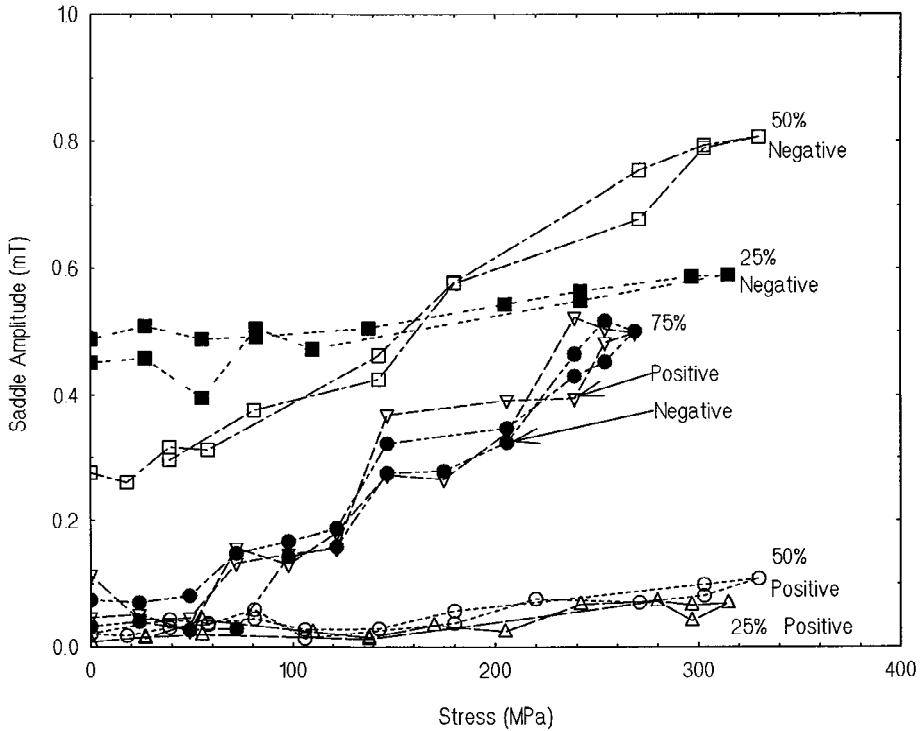


**Fig. 6.** Saddle amplitudes as a function of stress in the composite beam apparatus from 13-mm ball-milled defects in a field of 1.24 T in the after-cycle are plotted for the 25% defect for the positive ( $\Delta$ ) and negative ( $\blacksquare$ ), for the 50% defect for the positive ( $\circ$ ) and negative ( $\square$ ), and for the 75% defect for the positive ( $\nabla$ ) and negative ( $\bullet$ ) saddle amplitudes.

are: 1) the slope directions of the positive and negative saddles as a function of stress are all positive; 2) the rate of change of saddle amplitude as a function of stress for all three stress rigs is of the same order of magnitude, in contrast to the  $MFL_{pp}$  signal variations with stress, which demonstrate little correlation between the three different stress rigs; 3) the magnitude of the saddle amplitudes obtained from the positive saddle curves is greater than the corresponding negative saddle curves in the normal cycle; 4) no change in the saddle amplitudes was observed under compressive stress for bending stress applied in the axial direction in both the single and composite beams; 5) the magnitudes of the saddle amplitudes for the semicircular pipe section are approximately four times greater than those observed for the single and composite beams, and do not go to zero even with the largest application of compressive stress; and 6) there is a general increase in the positive and negative saddle amplitude slopes with increasing defect depth.

The slopes obtained from the after-cycle and opposite-cycle also demonstrate an increasing saddle amplitude slope with increasing defect depth, although increased intercepts for the 25 and 50% defects for the negative saddle amplitude variation are observed. This increase can be seen for the after-cycle in a comparison of Figs. 5 and 6. The sum of the positive and negative saddle amplitude slopes (the total saddle amplitude

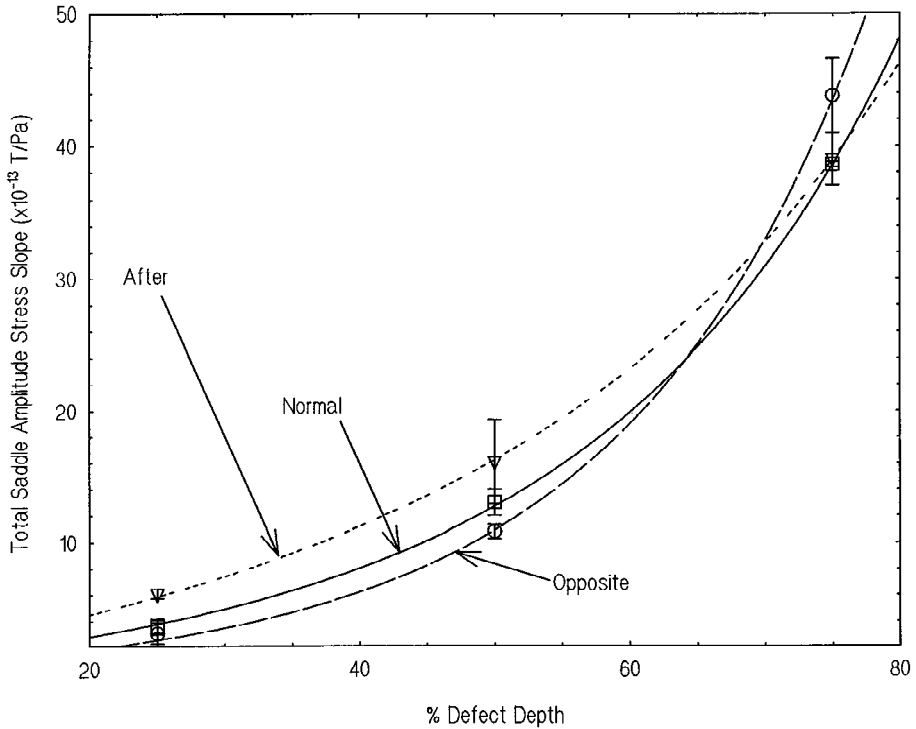


**Fig. 7.** The sum of positive and negative saddle amplitude stress slopes plotted as a function of % defect depth for the normal cycle (□), after-cycle, (▽) and opposite cycle (○) in the composite beam ( $B = 1.24 T$ ). The solid and dashed curves are lines to guide the eye.

slope) obtained from the three stress cycle results are plotted as a function of percent defect depth in Fig. 7.

The total saddle amplitude slope is plotted as a function of flux density for the after-cycle in Fig. 8. For all three cycles the results indicated an increasing total saddle amplitude with increasing flux density.

The stress concentration factor is a constant for constant defect depth and, therefore, may be related to the slope of the saddle amplitude variation with stress. However, for the zero-stress case, the radial flux leakage signal demonstrates a considerable increase with increasing defect depth [19, 20]. Therefore, to perform a comparison of the variation of the saddle amplitude with stress for different defect depths with calculated values of the stress concentration, it is necessary to normalize the stress-dependent saddle amplitude slopes by their respective zero-stress  $MFL_{pp}$  signals. A comparison of the normalized saddle amplitude slopes with the maximum and surface maximum stress concentrations obtained from finite-element calculations is shown in Fig. 9. The stress-dependent saddle amplitude slopes have been averaged over the three cycles, normalized by their respective zero stress  $MFL_{pp}$  signals, and scaled to the calculated maximum surface stress at 75% defect depth.

The normalized and scaled saddle amplitude slopes have been fitted in Fig. 9 with an

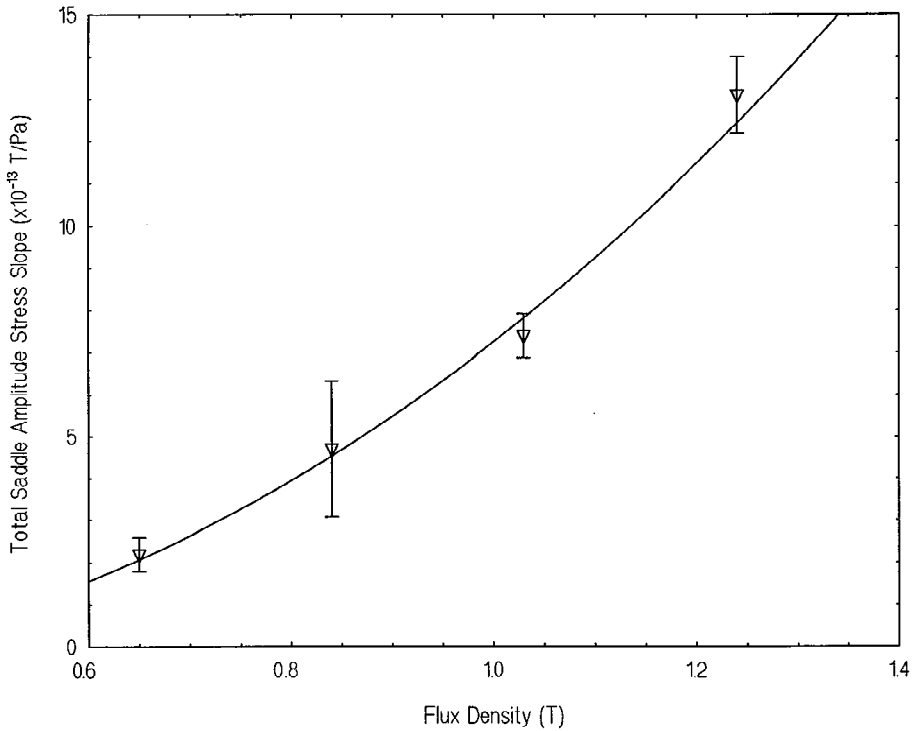


**Fig. 8.** Sum of positive and negative saddle amplitude stress slopes plotted as a function of pipe wall flux density for the after-cycle ( $\nabla$ ) in the composite beam ( $B = 1.24$  T). The solid curve is simply a line to guide the eye.

empirical formulation given by

$$A = a \sinh(bD), \quad (1)$$

where  $A$  is the sum of the positive and negative saddle amplitude slopes,  $D$  is the percent defect depth, and  $a$  and  $b$  are fitting parameters given by  $(a, b) = (0.71, 0.018)$ . Equation (1) holds in the limit of a 0% defect since the total saddle amplitude  $A$  goes to zero as the  $MFL_{pp}$  signal goes to zero.

The finite-element calculations indicate that both the maximum and surface maximum stress concentration are increasing functions of percent defect depth. Starting at 0% defect depth, the maximum stress concentration increases more rapidly than both the surface maximum and the normalized and scaled saddle amplitude slope values. Slower increases in the finite-element calculations are observed in the vicinity of 70%, which corresponds with the defect depth in the finite-element model where the radius of the defect reaches its maximum of 6.35 mm. After 90% the surface maximum concentration becomes the maximum stress concentration. The hyperbolic sine function, Eq. (1), coincides with the finite-element calculations above 75% defect depth and with the theoretical fractional change in stress concentration at 100% defect depth.

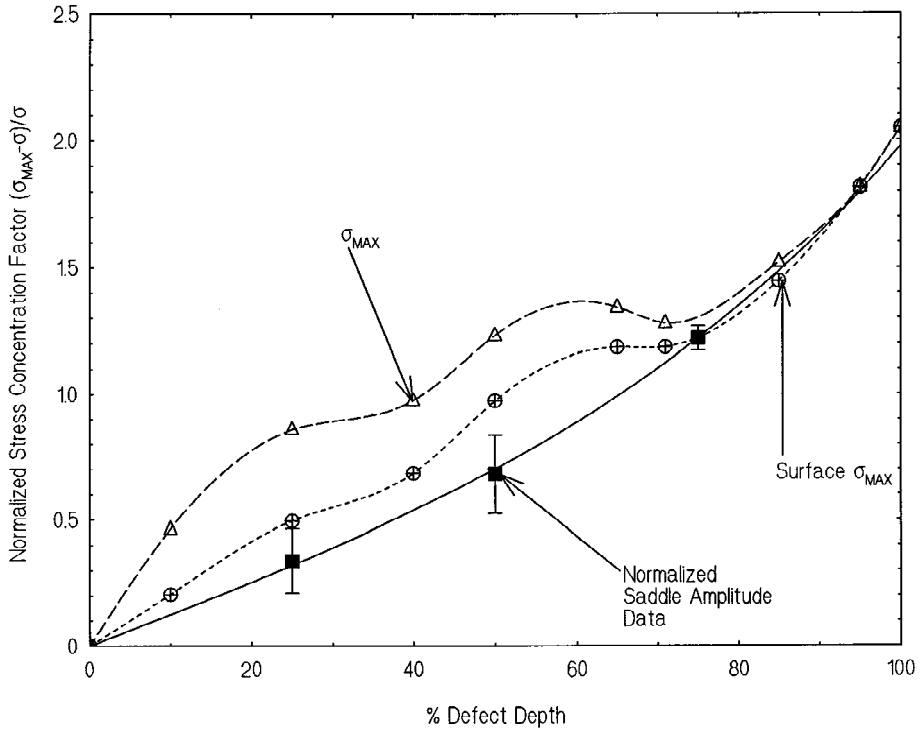


**Fig. 9.** Normalized change in maximum stress ( $\Delta$ ) and maximum surface stress ( $\oplus$ ) as a function of % defect depth as obtained from finite-element calculations. The total saddle amplitude stress slopes ( $\blacksquare$ ) for the composite beam normalized by their respective zero-stress MFL<sub>pp</sub> signals and averaged over the three different stress cycles have been scaled to the maximum surface stress (Surface  $\sigma_{MAX}$ ) finite-element calculations at 75% defect depth. The dashed lines are spline curves through the points obtained from the finite-element calculations and the solid line is a best fit of the empirical relation, Eq. (1).

## Discussion

### *Semicircular Pipe Section: MFL<sub>pp</sub> Measurements*

The application of a bending stress in the semicircular pipe section complicates the prediction of the magnetic flux leakage stress behavior of the pipe since, if the upper surface of the pipe with the near-side defect is under tensile stress, then the inner surface will be under compressive stress. A further complication in this system is the direction of the magnetic easy axis with respect to the direction of the applied stress. The magnetic easy axis is at  $90^\circ$  to the direction of the applied stress, and, therefore, the magnetic properties of the pipeline steel are different [21] from those where the stress and easy axis are aligned in the same direction [22]. Geometric properties of the semicircular pipe stress rig also may play a role in affecting the stress-dependent variation of the MFL<sub>pp</sub> signal, since the radius of curvature and therefore the length of the flux path in the semicircular pipe section changes as a function of stress with respect to the

fixed length of the magnetizer. Furthermore, different levels of pipe wall flux density at equivalent stress levels for increasing and decreasing applied stresses may arise because of hysteretic flux coupling in the hinged finger–semicircular stress system. This may explain the severe hysteresis observed in the radial  $MFL_{pp}$  signal for the semicircular pipe section under tensile stress shown in Fig. 3.

The application of a hoop-bending stress that is either tensile or compressive results in an overall decrease of the  $MFL_{pp}$  signal for either surface tensile or surface compressive applied stress. However, there is an initial increase of the  $MFL_{pp}$  signal under a surface tensile stress of 50 MPa. This may be attributed to the presence of a residual compressive surface stress present within the pipe. This suggestion is supported by spring-back measurements observed when the pipe section was cut in half [22].

### *Stress-Dependent Saddle Amplitude: Stress Concentration Factors*

The variation of the  $MFL_{pp}$  signal with stress appears to be associated primarily with the bulk effects of stress [9], [11]–[13] and pipe wall flux density [9, 13] on the magnetic properties of steel in the general vicinity of the defect. However, we propose that the double-peak feature in the  $MFL_{pp}$  signal and the variation of the saddle amplitude with stress is associated with the near-surface variation of stress in the immediate vicinity of the defect, which acts as a local stress raiser [17].

Measurements of the  $MFL_{pp}$  signal with almost uniform bulk stress in the composite beam stress rig indicate an increase of the  $MFL_{pp}$  signal with increasing uniaxial tensile stress [9, 13]. Similarly, the variation of the saddle amplitude as a function of stress at the near-side surface of the defect demonstrated the same positive dependence. The rate of change of the saddle amplitude as a function of stress was also of the same order of magnitude in all three apparatus. Since it is the surface stress in all three apparatus that is monitored, we associate the saddle amplitude behavior as a function of stress with the corresponding variation of surface stress in the pipeline steel in the vicinity of the defect.

Normalization of the stress-dependent saddle amplitude variation by the stress-dependent  $MFL_{pp}$  slope for the case of the composite beam is shown in Table 1. The results indicate that the saddle amplitude increases with defect depth faster than the stress-dependent  $MFL_{pp}$  signal. Also shown in Table 1 are the positive and negative saddle amplitude slopes for the single beam normalized by the stress-dependent  $MFL_{pp}$  slope for the 50% defect. The values for the normalized saddle amplitude slopes obtained in this manner are more than twice those obtained for the 50% defect in the composite beam. Normalization of the semicircular pipe section stress-dependent saddle amplitude by the corresponding  $MFL_{pp}$  stress-dependent signal generates a nonlinear stress variation since the  $MFL_{pp}$  signal varies nonlinearly over the applied tension–compression stress cycle. As was shown elsewhere [9, 13], the single and composite beams demonstrate a compressive stress dependence, while no saddle amplitude is observed in this applied stress region. These results demonstrate that the variation of the  $MFL_{pp}$  signal as a function of the bulk stress effect cannot explain the observed stress-dependent variation of the saddle amplitude. Furthermore, the slope of the saddle amplitude as a function of measured surface stress for the 50% defect in the three different stress rigs, two of which are under a bending surface stress, are all of the same order. These points indicate

that the saddle amplitude can only be associated with the nonuniform stress effects that appear near the surface of the pipe in the vicinity of the defect.

The behavior of the magnitude of the saddle amplitude for the semicircular pipe section, which is greater than that observed in the single and composite beams and does not go to zero with the application of compressive stress, may arise due to a number of differences between the two systems. These differences include the direction of the magnetic easy axis, which is axial for this particular pipe [22] and, therefore, is at  $90^\circ$  to the direction of applied stress for the semicircular pipe section and parallel to the direction of applied stress in the composite beam. The different directions of the easy axis may result in different stress-dependent behavior of the magnetization in the vicinity of the defect [23]. The observation that different levels of magnetization affect the magnitude of the measured saddle amplitude is supported by the differences observed in the composite beam results in the magnitude of the negative saddle amplitude for the 50% defect between the normal cycle (Fig. 5) and the after-cycle (Fig. 6). These differences may be associated with the effect of the order in which field and stress are applied, i.e., hysteresis [24]. Greater differences between the three cycles may be expected in the lower flux density regions investigated here, where hysteresis is greater, than when the magnetization in the pipe wall approaches saturation.

The variation of the saddle amplitude slope as a function of flux density, as shown for the after-cycle in the composite beam in Fig. 8, may be expected to saturate at higher flux densities. Therefore, a limit to the increase in the radial  $MFL_{pp}$  signal is expected at higher flux densities, which were not investigated here.

The effect of stress concentrations arising around hole defects has been described in the literature [8, 18]. In this case the maximum stress arises at the edges of the circular defect whose tangentials are parallel to the nominal applied tensile stress direction [8, 18]. The maximum stress concentration achieved here for a two-dimensional through-hole is three times that of the nominal stress [7].

The finite-element calculations verified that the surface stress concentration is an increasing function of increasing defect depth. The simple modeling used to simulate the stress in the vicinity of a blind-hole pit introduced several artifacts and uncertainties into the finite-element calculations. In particular, the through-thickness uniform tensile stress was only an approximate simulation of the composite beam stress rig where the stress through the thickness of the pipe wall varied by 30%, and was not an accurate simulation for the bending stress rigs. Furthermore, the application of a fixed radius of curvature for the generation of the simulated ball-milled defect resulted in an increasing defect radius with increasing defect depth up to 71%, where the full diameter of the defect was attained. The changing radius of the defect with defect depth also may have introduced an error as a result of the changing defect size with respect to the fixed mesh size. After 71% the simulated round-bottomed defect has a constant radius with cylindrical sides. This could explain the local minimum reached at 71% defect depth in the normalized change in stress as a function of defect depth curves obtained from the finite-element calculations.

The radial  $MFL_{pp}$  signal increases very rapidly with depth beyond 75% of the through-wall thickness [19, 20]. In order to account for this strong variation in the  $MFL_{pp}$  signal and its affect on the saddle amplitude values, the saddle amplitude slopes were normalized by their respective composite beam radial  $MFL_{pp}$  signals. The normalized saddle

amplitude slope still demonstrated an increase with increasing defect depth, as is seen in Fig. 9. This indicates that the stress dependence of the saddle amplitude slope increases more rapidly than the  $MFL_{pp}$  signal with increasing defect depth. Therefore, this increase may be associated with the stress concentration in the vicinity of the defect, which, from the finite-element calculations, also demonstrates an increase with increasing defect depth.

The variation of the normalized total saddle amplitude slope is in qualitative agreement with the calculated surface stress concentration variation with increasing defect depth. The smaller values of the normalized-scaled saddle amplitude slopes may be a result of the 30% through-wall variation of the stress that reduces the stress concentration in the actual composite beam. A similar reduction in the stress concentration has been observed for a defect under a bending stress [17], which is a 200% through-wall variation of stress.

The finding that the total saddle amplitude contribution to the MFL signal increases with increasing defect depth is in agreement with previous measurements which indicate that the normalized change in the  $MFL_{pp}$  signal with stress is greater for deeper defects [9, 13]. If the saddle amplitude is associated with the defect as a local stress raiser, the surface stress conditions arising from the presence of the defect may be considered as an important component of the  $MFL_{pp}$  signal for uniaxial field and stress conditions. This is particularly true for the hoop-bending stress in the semicircular pipe section where the sum of the positive and negative saddle amplitudes for a 50% defect are 6% of the total flux leakage signal.

The observed correlation between stress concentration and the saddle amplitude may provide a method for monitoring surface stress concentrations in other defect geometries.

## Conclusions

Investigations of the stress-dependent magnetic flux leakage (MFL) signal from blind-hole defects for uniaxial field and stress in pipeline steel indicated that the saddle amplitude feature in the radial MFL signal increased approximately linearly with increasing tensile surface stress and decreased, or did not exist, for increasing compressive surface stress. The rate of increase was of the same order of magnitude for the 50% defect in the three stress rigs investigated and was only dependent upon the nominal surface stress of the pipeline steel within which the defect was located. Finite-element calculations confirmed that the stress concentration in the surface vicinity of the defect is an increasing function of defect depth. These results supported the hypothesis that the stress-dependent saddle amplitude behavior may be associated with stress concentrations at the defect near the surface of the pipe.

*Acknowledgment.* This research was supported by the Natural Sciences and Engineering Research Council of Canada, Pipetronix, and the Gas Research Institute.

## References

1. D. L. Atherton. *Oil & Gas J.* **87**(32):52–61 (1989)
2. D. L. Atherton. *Oil & Gas J.* **84**(43):86–89 (1986)
3. D. L. Atherton, A. Dhar, C. Hauge, and P. Laursen. *Oil & Gas J.* **90**(27):81–83 (1992)
4. P. Laursen and D. L. Atherton. *British J. Non-Destructive Testing* **34**(6):285–288 (1992)
5. P. Laursen. “Effects of Line Pressure Stress on Magnetic Flux Leakage Patterns,” M.Sc. Thesis, Queen’s University, Kingston (1991)
6. C. Hauge. *Effects of Line Pressure on Axially Excited Magnetic Flux Leakage Patterns*, M.Sc. Thesis, Queen’s University, Kingston (1995)
7. C. Hauge and D. L. Atherton. *Oil & Gas J.* **94**(12):92–96 (1996)
8. R. E. Peterson. *Stress Concentration Factors*, John Wiley & Sons, New York, p. 110 (1974)
9. T. W. Krause, R. M. Donaldson, R. Barnes, and D. L. Atherton. *NDT&E Int.* **29**(2):79–86 (1996)
10. In: *Metals Handbook*, 8th Edition, Vol. 10, ASM (1977)
11. R. Barnes and D. L. Atherton. *NDT&E Int.* **26**(1):3–6 (1993)
12. R. Barnes. *Comparison of the Effects of Surface and Uniform Stresses on Magnetic Flux Leakage Signals*, M.Sc. Thesis, Queen’s University, Kingston (1993)
13. D. L. Atherton, R. Barnes, R. M. Donaldson, T. W. Krause, and R. W. Little. *Effects of Line Pressure Stress, Magnetic Properties and Test Conditions on Magnetic Flux Leakage Signals*, Annual Report to Gas Research Institute (May 1993–April 1994), GRI Contract # 5093-260-2605
14. D. L. Atherton, C. Hauge, T. W. Krause, A. Pattantyus, Donaldson, and R. Barnes. *Effects of Line Pressure Stress, Magnetic Properties and Test Conditions on Magnetic Flux Leakage Signals*, Annual Report to Gas Research Institute (May 1994–April 1995), GRI Contract # 5093-260-2605
15. D. L. Atherton and P. Laursen. “MFL signals: the shape of things to come,” *Proc. 7th Int. Pipeline Pigging Conference*, Houston, 13–16 Feb. (1995)
16. D. L. Atherton. *Pipes & Pipelines Int.* **40**(1):9–13 (1995)
17. L. Clapham, T. W. Krause, H. Olsen, B. Ma, D. L. Atherton, and T. M. Holden. *J. Strain Anal.* **29**(4):317–323 (1994)
18. R. C. J. Howland. *Phil. Trans. Roy. Soc. (London) A* **229**:49–86 (1929–30)
19. D. L. Atherton. *British J. NDT* **30**(3):159–162 (1988)
20. D. L. Atherton and M. G. Daly. *NDT Int.* **20**(4):235–238 (1987)
21. T. W. Krause, A. Pattantyus, and D. L. Atherton. *IEEE Trans. Magnetics* **31**(6):3376–3378 (1995)
22. L. Clapham, T. W. Krause, H. Olsen, B. Ma, D. L. Atherton, P. Clark, and T. M. Holden. *NDT&E Int.* **28**(2):73–82 (1995)
23. T. W. Krause, J. M. Makar, and D. L. Atherton. *J. Magn. Magn. Mat.* **137**:25–34 (1994)
24. D. L. Atherton and T. Sudersena Rao. *J. Appl. Phys.* **62**(2):2914–2917 (1987)